

# Force and Moment Constraints of a Curved Surface Gripper and Wrist for Assistive Free Flyers

Matthew A. Estrada, Hao Jiang, Bessie Noll,  
Elliot Hawkes, Marco Pavone, Mark R. Cutkosky

**Abstract**—Free-flying robots have the potential to autonomously fulfill a wide range of tasks involving manipulation of objects in space. In this paper we study the design of a wrist mechanism for free-flying robots that are equipped with an adhesive gripper for attaching to objects and surfaces. The wrist and gripper allow the robots to apply moments in addition to forces, which increases their versatility for object manipulation. We apply grasp optimization to establish limitations on the forces/moments that the wrist can impart, subject to adhesion capabilities. Building on these results, we present considerations for tuning a passive wrist mechanism, or controlling an active wrist, to broaden the range of forces and moments that the robot can exert. Our theoretical insights and wrist designs are validated in simulations and on a planar micro-gravity test bed.

## I. INTRODUCTION

In the near future it is anticipated that free-flying robots will assist astronauts in manipulating objects in and around space vehicles [1]–[3]. In this context, manipulators designed to grasp the surfaces of objects and structures have been of recent interest [4]–[7] and stand to transform large swathes of structures, such as external hulls of spacecraft or solar panels, into suitable attachment sites. Broadening attachment choices would simplify operations such as docking maneuvers, orbital debris removal, and on-orbit servicing, where pre-installed features often dictate current procedures. Some applications demand a more versatile gripping capability, such as capturing uncooperative targets [8], [9] or anchoring onto objects that are not man-made [10].

To this end, we previously explored using a flexible gripper that employs a gecko-inspired adhesive to capture curved and possibly rotating objects [11]. However, in order to manipulate objects conveniently, a free-flying robot should also be able to apply rotations or moments using a wrist. In this paper we show that a free-flying robot with an adhesive gripper and an active wrist with torque control can increase the range of possible object acquisitions and manipulations beyond those possible with a passive, compliant wrist.

We present a new adhesive gripper that features a palm such that it can apply moments to objects while also applying both normal and shear forces. We model the gripping

M. A. Estrada, H. Jiang, B. Noll, E.W. Hawkes, and M. R. Cutkosky are with the Mechanical Engineering Dept., Stanford University, Stanford, CA 94305. M. Pavone is with the Aeronautics and Astronautics Dept., Stanford University, Stanford, CA 94305. E.W. Hawkes is with the Mechanical Engineering at University of California, Santa Barbara, Santa Barbara, CA 93106.

Emails: {estrada1, jianghao, bnoll, ewhawkes, cutkosky, pavone}@stanford.edu

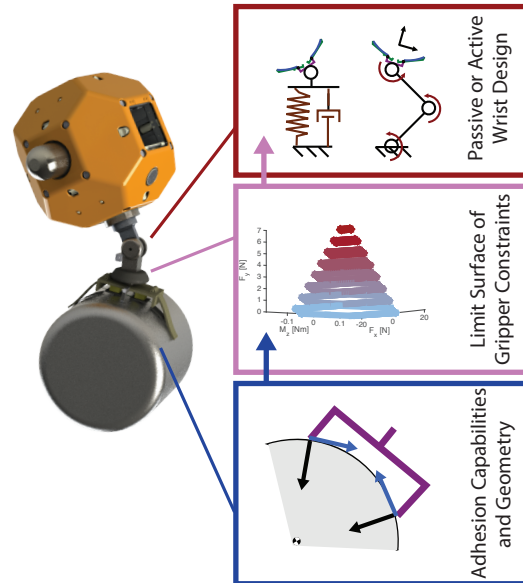


Fig. 1. Free flyer SPHERES robot [2] is shown grasping an object with a curved surface gripper. In this paper, adhesion capabilities and gripper geometry are used to calculate the forces and moments able to be applied by the gripper. These limits are then used to investigate passive wrist tuning and the potential advantages of active control.

constraints and show how they affect the design and control of the wrist. The analysis begins from surface interaction forces and works back towards the robot, as depicted in Fig 1; using a free body diagram of the gripper design adhesion limitations are mapped into a force-moment space. Keeping reaction forces within this safe region becomes the ultimate goal of wrist design. To validate the model, we present simulations and experiments on a free-floating platform, approximating a two-dimensional micro-gravity environment.

## II. CURVED SURFACE GRIPPER MODEL

### A. Background and related prior work

A starting point for the analysis presented here is to model the force and moment capabilities of the new gripper as a function of contact forces, including adhesive forces. The analysis draws upon analyses of grasping with robot hands and force balancing for the feet of climbing robots.

Grasp force optimization is a well-studied subject. In general the problem is posed in terms of external and internal forces, using either linear or nonlinear optimization to relate

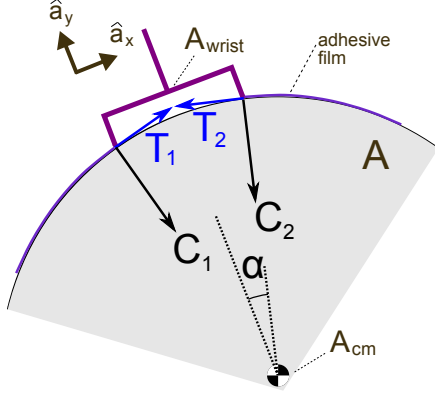


Fig. 2. Planar free body diagram of forces on an object of locally uniform curvature. Adhesive forces,  $T_1, T_2$  act tangential to the surface; compressive forces,  $C_1, C_2$  act normal to the surface.  $\alpha$  is half of the angle subtended by the palm. Coordinate frames embedded in the object and gripper are  $A_{cm}$  and  $A_{wrist}$ , respectively. The gripper is assumed rigidly connected to the object until maximum adhesive forces are exceeded.

the two [12]–[15]. A related problem arises when adhesives are used for climbing or perching. Examples include optimizing the force balance on the feet of a quadrupedal climber [16], [17] or the forces available from collections of directional adhesive pads [18].

### B. Force/Moment Limitations

In the present case we refer to gripper capabilities as a region of attainable forces and moments exerted on a target object. This region is a function of gripper geometry and the maximum load each adhesive can withstand. For the purposes of this paper we are interested primarily in the adhesive capabilities of the gripper, essential when it is pulling on an object to acquire or manipulate it. In the following development, we ignore the case of pushing an object with the gripper, although this extension to the force/moment limit surface is straightforward.

We express 2D net force and moment as a set of linear matrix equations with inequality constraints; four internal reaction forces sum to net forces along two directions and one moment balance about a third.

### C. Free Body Diagram

A free body diagram of the forces exerted by the curved surface gripper is shown in Fig. 2. Four possible forces are exerted by the gripper: shear adhesion forces  $T_1, T_2$  act tangential to the object’s surface. Compression forces  $C_1, C_2$  act normal to the surface. Parameter  $\alpha$  denotes the half angle subtended by the palm in contact with the object.

Net force and moment about point  $A_{cm}$  can be expressed as a column vector,  $F_{cm}$ , expressed in the reference frame aligned with body A. Similarly, the magnitudes of internal reaction forces can be arranged in a column vector:

$$F_{cm} = \begin{bmatrix} \Sigma F_x \\ \Sigma F_y \\ \Sigma M_z \end{bmatrix}, x = \begin{bmatrix} \|\vec{T}_1\| \\ \|\vec{T}_2\| \\ \|\vec{C}_1\| \\ \|\vec{C}_2\| \end{bmatrix} \quad (1)$$

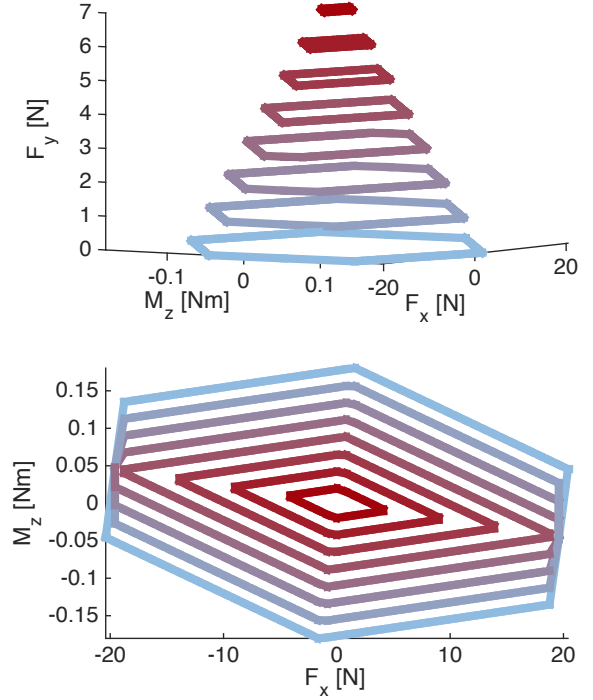


Fig. 3. Limit surface for  $\mathcal{L}_{wrist}$  for  $\alpha = 11.4^\circ$ ,  $r = 0.11$  m, and a maximum adhesion of 20 N on each adhesive strip. All forces and moments enclosed within the surface are within the adhesion’s capabilities. Lines of constant  $F_y$  are plotted in increments of 1 N. The gripper is capable of exerting compressive forces, though we restrict our focus to “adhesive manipulations” where  $\Sigma F_y > 0$  for the purposes of this development.

The relation between net force and moment exerted on the object from these reaction forces is posed as a matrix equation:

$$F_{cm} = G_{cm}x, \quad (2)$$

where  $G_{cm}$  denotes the contribution each force vector has on the force and moment balance. In this 2D case,  $G_{cm}$  is a  $3 \times 4$  matrix, as there are three degrees of freedom (DOF) and four force vectors, specifically

$$G_{cm} = \begin{bmatrix} \cos \alpha & -\cos \alpha & \sin \alpha & -\sin \alpha \\ \sin \alpha & \sin \alpha & -\cos \alpha & -\cos \alpha \\ -r_1 & r_2 & 0 & 0 \end{bmatrix} \quad (3)$$

where  $r_1$  is a moment arm from  $A_{cm}$  to the contact point at  $C_1$ ; the right contact follows similarly.

The net forces and moments exerted on the object are given by  $F_{cm}$ , taken at  $A_{cm}$ . Note that  $F_{cm}$  consists of mixed units, denoting two forces and one moment for the purposes of this paper.

### D. Convex Set of Achievable Forces/Moments

The net forces and moments that can be exerted by the gripper, about point  $A_{cm}$ , without overloading adhesive capabilities, are any force/moment vector lying within the convex set  $\mathcal{L}_{cm}$ :

$$\mathcal{L}_{cm} := \{F_{cm} \mid F_{cm} = G_{cm}x \mid 0 \leq x \leq x_{max}\}. \quad (4)$$

The nonzero inequality constraint ensures that compressive forces only push while adhesive forces only pull. The upper bound,  $x_{max}$ , encodes adhesion limitations. Compressive force limitations at each contact point (to prevent structural damage) can be imposed as well.

The boundary between forces/moments within the convex set and those that will exceed the adhesive's capabilities is called the gripper's "limit surface," depicted in Fig. 3. As noted earlier, we restrict our focus to "adhesive manipulations" where  $\Sigma F_y > 0$  for the purposes of this development.

### E. Force Optimization

One can pose a simple convex optimization problem in order to find the largest force the gripper is able to exert with given adhesion capabilities and geometry. For some objective  $\beta$ , we write:

$$\begin{aligned} & \underset{x}{\text{maximize}} && \beta \\ & \text{subject to} && F_{cm} = G_{cm}x \\ & && 0 \leq x \leq x_{max} \end{aligned} \quad (5)$$

For instance, we can find the largest force able to be exerted on an object in the  $\hat{a}_x$  direction by choosing  $\beta = \Sigma F_x$ . Similarly, we can find the largest force in the  $\hat{a}_x$  direction without inducing a linear acceleration in the  $\hat{a}_y$  direction, nor a rotation about  $\hat{a}_z$ . In this case, we would use the same objective and add two additional constraints, namely:  $\Sigma F_y = 0$ ,  $\Sigma M_z = 0$ .

### F. Calculating Adhesive Load from Net Forces

Equation 2 calculates net forces from specified reaction forces in the free body diagram. Calculating the magnitude of adhesive and compressive loads from net forces represents an under-constrained problem: calculating four force magnitudes from three net force/moments. This extra degree of freedom is due to the fact that  $G_{cm}$  has a nullspace:

$$\mathcal{N}(G_{cm}) = \begin{bmatrix} 1 \\ 1 \\ \tan \alpha \\ \tan \alpha \end{bmatrix}$$

The forces can thus be calculated via a constrained, least-norm problem with a non-negative constraint on  $x$ . Physically, the minimization is asserting that no unnecessary internal reaction forces acting within  $\mathcal{N}(G_{cm})$  are present.

### G. Shifting the Point of applied Forces

To calculate the set of net forces that can be applied to the object at a different point, one can perform a transformation:

$$F_{wrist} = \begin{bmatrix} 1 & 0 & 0 \\ 0 & 1 & 0 \\ \vec{r}^{wrist/cm} \cdot \hat{a}_y & 0 & 1 \end{bmatrix} F_{cm}. \quad (6)$$

This transformation takes into account that forces in the  $\hat{a}_x$  direction will be acting with a different moment arm when moments are calculated about a different point. Here, we assume that the translation between the two points only occurs along the  $\hat{a}_y$  axis. For generality, point  $A_{wrist}$  is taken

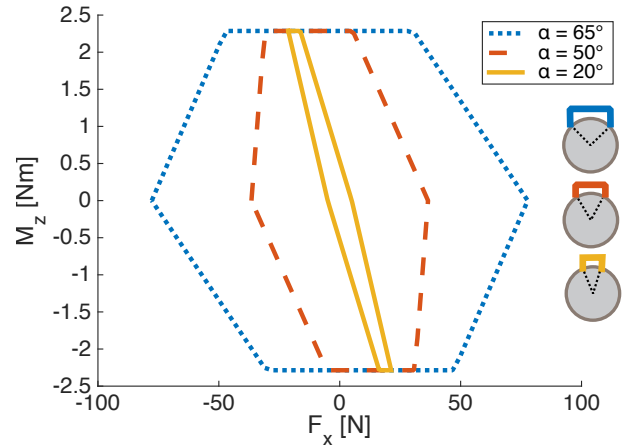


Fig. 4. The model presented in section II can be used to assess different gripper designs. Space enclosed by  $\mathcal{L}_{cm}$  is depicted above as  $\alpha$ , the half angle subtended by the gripper's palm, varies. For visualization, we plot a 2D slice of the limit surface, where  $\Sigma F_y = 0$ .

to be at the surface of the cylindrical object, a distance  $r$  from the center of mass (an actual gripper would be slightly more offset). For analysis, point  $A_{wrist}$  is considered to be part of the object's rigid body since it does not deflect with respect to any point on the object once grasped.

Denoting the matrix in Eq. 6 as  $T^{wrist/cm}$ , one can analogously map entire force/moment convex spaces:

$$\mathcal{L}_{wrist} = T^{wrist/cm} \mathcal{L}_{cm} \quad (7)$$

### H. Effects of Parameters

Varying parameters of the model leads to useful insights on the forces potential gripper designs can exert on an object. For instance, varying  $\alpha$  allows us to explore the benefits of a gripper that spans a larger arc on the surface of the object, depicted in Fig. 4. For visualization, we take a slice of the limit surface, assuming  $\Sigma F_y = 0$ . These net forces at  $F_{cm}$  are synonymous with net accelerations of point  $A_{cm}$ , just scaled by mass/inertia.

As  $\alpha$  increases, the space of allowable forces grows, since compressive forces are oriented more favorably, able to act both normal and tangential to the gripper frame. The shape also becomes less diagonal as  $\alpha$  increases, meaning the gripper's ability to exert tangential acceleration and rotational accelerations becomes less coupled.

Of course, varying  $\alpha$  is only one example of investigating different gripper designs. Varying wrist position or modeling configurations with asymmetric adhesive capabilities also offer interesting trade-offs. A designer may concentrate more adhesive on one side of the gripper to handle large tangential forces at the price of reduced normal forces.

## III. PASSIVE WRIST TUNING

An important goal of passive wrist design for a force-limited gripper is to keep forces within the adhesive's capabilities. In other words, the set of exerted forces must lie within the limit surface derived in section II. Without knowing what combination of loads the wrist will experience

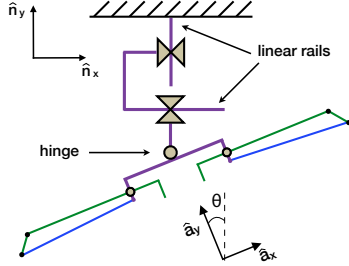
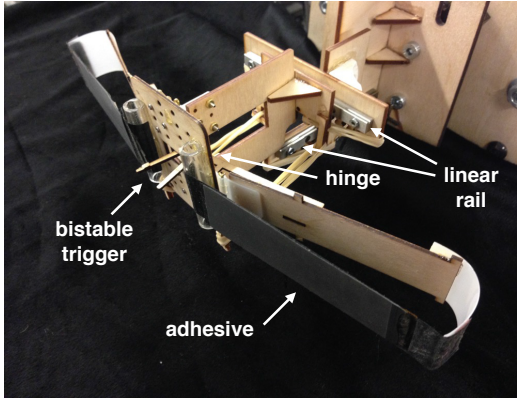


Fig. 5. Gripper and wrist designed to have compliance in three orthogonal degrees of freedom. Two linear rails are mounted allowing deflection in the  $\hat{n}_x$  and  $\hat{n}_y$  directions. The gripper is mounted on a hinge, allowing rotation about the  $\hat{n}_z$  axis.

at each instant a priori, the wrist must be soft enough that the maximum force will never exceed the limit surface constraints.

We present a gripper and wrist with compliance in three orthogonal directions, two linear and one rotational, depicted in Fig. 5. A linear slider provides compliance along the  $\hat{n}_y$  direction, with another slider attached in series to give compliance in the  $\hat{n}_x$  direction. The gripper is attached at the distal end via a pin joint, providing a rotational compliance about the  $\hat{n}_z$  axis.

For a passive wrist, ensuring that reaction forces remain within a gripper's limit surface requires tuning the stiffness and damping at each joint. We assume the mass of the gripper and wrist is negligible, and that a simple linear, stiffness and damping are present at each joint of the wrist. The force felt at the gripper, expressed in the end effector's reference frame, is a function of the joints' deflection from its resting state,  $\Delta q = [\delta x \ \delta y \ \delta \theta]^T$  and joint velocity  $\dot{q} = [\dot{x} \ \dot{y} \ \dot{\theta}]^T$ :

$$F_{applied} = J(\theta) * (-K\Delta q - B\dot{q}) \quad (8)$$

Where the stiffness and damping matrices are represented as  $K = \text{diag}(k_x, k_y, k_\theta)$  and  $B = \text{diag}(b_x, b_y, b_\theta)$ , respectively. The wrist's Jacobian is denoted  $J(\theta)$ :

$$J(\theta) = \begin{bmatrix} \cos \theta & -\sin \theta & 0 \\ \sin \theta & \cos \theta & 0 \\ 0 & 0 & 1 \end{bmatrix} \quad (9)$$

The objective in tuning depends on the intended task: dynamic uses will rely heavily on the level of damping, fine

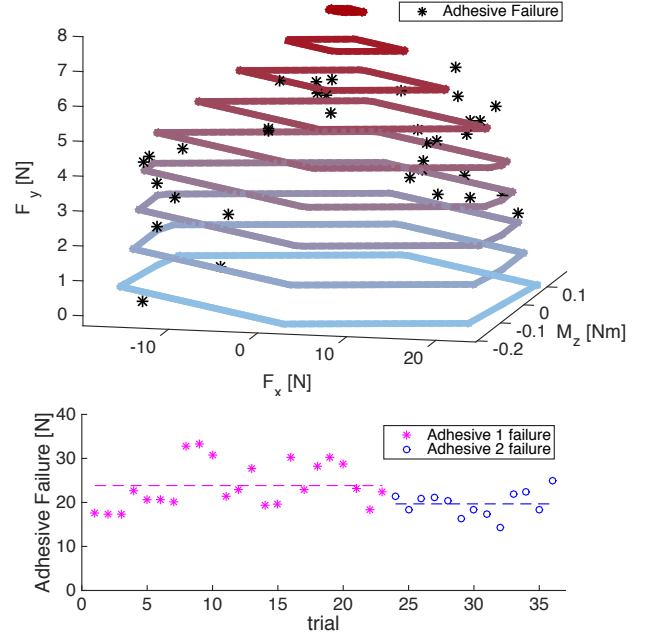


Fig. 6. Limit surface of  $\mathcal{L}_{wrist}$  for the curved surface gripper shows the attainable forces and moments at the wrist (point  $A_{wrist}$ ) given the adhesive's capabilities. Axes are resultant forces in the  $a_x, a_y$  direction, and the moment about the  $a_z$  direction. Data from pull-off tests (\*) are shown along the limit surface. The asymmetry of the envelope is due to the two adhesive pads having slightly different capabilities. Calculated adhesive load is shown below for both adhesive pads.

manipulations may require a nonlinear stiffness that acts rigid under modest loads and deflects once overloading is near. For dynamic or uncertain applications, sweeping a dynamic simulation over expected conditions provides an assessment of wrist performance, as done in [19], [11]. An exhaustive simulation of spring and damping coefficients is done in section V-C, to find the best case scenario of a passive wrist with linear compliance and damping.

#### IV. ACTIVE WRIST CONTROL

Whereas a passive wrist must be designed for the worst-case combination of forces and moments, an active wrist needs to contend only with the specific combination of forces and moment that are in effect at each instant. In other words, an active wrist may act at the edge of the limit surface, rather than conservatively within it.

Applying forces consistently near the adhesive limits is useful for dynamic manipulations where large interaction forces are desired. An example scenario is catching an uncooperative target tumbling through space – a free flyer robot must absorb the kinetic energy corresponding to the relative motion of the robot and object.

Specifically, if  $\vec{F}_{cm}$  is the net force applied at the object's center of mass, a possible control strategy becomes:

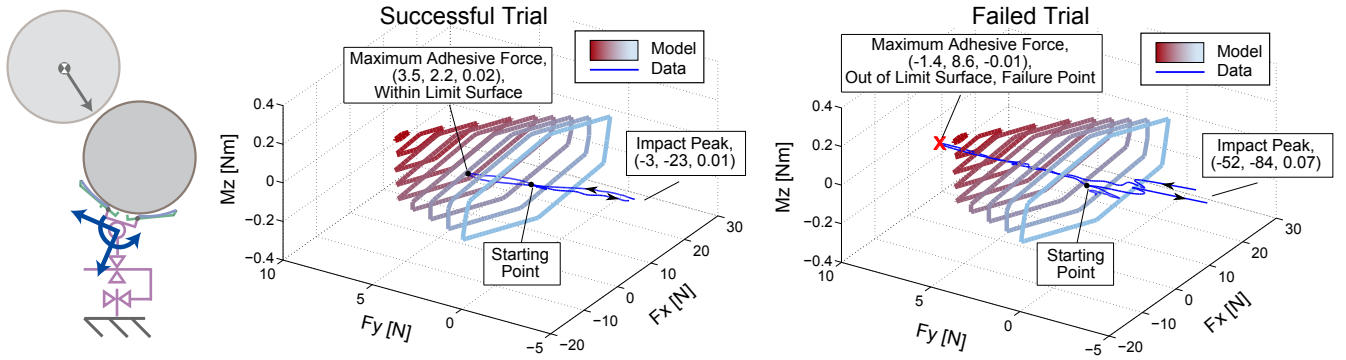


Fig. 7. The force felt at the wrist’s distal joint during a dynamic catch is shown in blue. A successful grasp is shown to stay within the limit surface while a failed grasp breaks away from the gripper when it exceeds the adhesive’s capabilities, marked in red. For both trials, impact peaks produced high compressive forces ( $F_y < 0$ ) which did not appreciably load the adhesives but affected the structure of the gripper. These compressive peaks are out of the view in the presented plots, but the magnitude is noted for each.

$$\begin{aligned}
 & \underset{F_{cm}}{\text{maximize}} && \beta \\
 & \text{subject to} && F_{cm} = -\beta \begin{bmatrix} L_x \\ L_y \\ H_z \end{bmatrix} \\
 & && F_{cm} \subseteq \mathcal{L}_{cm}
 \end{aligned} \quad (10)$$

where  $L_x, L_y, H_z$  denote the object’s linear/angular momentum about the  $\hat{a}_x, \hat{a}_y, \hat{a}_z$  directions, with  $H_z$  calculated about  $A_{cm}$ . Here, after calculating the net force to be applied at the object’s center of mass, we calculate  $F_{wrist} = T^{wrist/cm} F_{cm}$  for the corresponding force to apply at the wrist. Since we are optimizing for the largest interaction forces, the optimal input will lie on the gripper’s limit surface.

Pushing in proportion to the object’s momentum is proposed in order to bring all components of momentum to rest simultaneously, though this would require an estimation of the target object’s mass properties and incoming state [20]. Control laws also can be formulated using the velocity of the point of attachment, which could be calculated by encoders within the arm’s joints.

## V. EXPERIMENTAL RESULTS

We present experiments and simulations to confirm the limit surface and its use for object manipulation. First, the limit surface modeled in section II is compared to the empirical limits of an adhesive gripper. Next, force measurements of a dynamic catch with the passive gripper introduced in section III are shown for both a successful and failed grasp. Finally, a simulation shows the potential performance improvement an active gripper can offer with the control proposed in section IV.

### A. Limit Surface Verification

The gripper was subjected to failure tests under different loads to verify the suitability of the model presented in section II. Quasi-static, load-bearing experiments for the curved surface gripper show empirical points of adhesive failure around the limit surface in Fig. 6. The gripper was rigidly mounted to an ATI-Gamma SI-32-2.5, six axis

force/torque sensor (accuracy:  $\pm 0.05$  N), which measured forces at 1000 Hz. The gripper was attached to a cylindrical object (23 cm diameter) before being loaded to failure. The surface of the object was covered with paper to reduce the adhesion such that gripper forces could easily be overcome by hand.

The gripper was loaded in a variety of conditions until the adhesive failed and the object was wrenched free from the gripper. The maximum force/moment exerted just prior to failure is depicted by each data point in Fig. 6. Values  $\alpha = 11.4^\circ$  and  $r = 0.115$  m were measured for the geometry of this gripper.

For each measurement, an adhesive load was calculated as described in section II-F. The adhesive load at failure is shown at the bottom of Fig. 6. The performance of each adhesive was slightly unequal, with adhesive 1 supporting up to 24.0 N, and adhesive 2 supporting up to 19.4 N. These maximum forces were used to generate the limit surface shown with the data (recall from section II-C maximum adhesion is set in the inequality constraint,  $x \leq x_{max}$ ).

The failure results presented here agree with the limit surface model in Section II-D. While geometry and adhesive capability are kept constant here, grasping with shear adhesion is modeled and verified for different values of constant and compound curvatures in related work [21].

### B. Force Profile of Dynamic Catch

The force profile was recorded for failed and successful, dynamic grasps. The dynamic catches were performed on a free floating platform to approximate a 2D micro-gravity environment. The 23 cm diameter target object had a mass of 1.55 kg and inertia of 0.013 kg·m<sup>2</sup>, identical to that used in [11]. The stiffnesses of the gripper were measured to be  $k_x = k_y = 250$  N/m,  $k_\theta = 0.125$  Nm, and damping  $b_x = b_y = 2$  Ns/m,  $b_\theta = 0.02$  Nms.

Traces from a typical success and failure are shown in Fig. 7. The incoming velocities for each trial were measured as:

$$\vec{v}_{success} = \begin{bmatrix} 0.5 \frac{m}{s} \hat{n}_x \\ 0.5 \frac{m}{s} \hat{n}_y \\ 0.3 \frac{rad}{s} \hat{n}_z \end{bmatrix}, \quad \vec{v}_{fail} = \begin{bmatrix} 0.4 \frac{m}{s} \hat{n}_x \\ 1.3 \frac{m}{s} \hat{n}_y \\ 0 \frac{rad}{s} \hat{n}_z \end{bmatrix}.$$

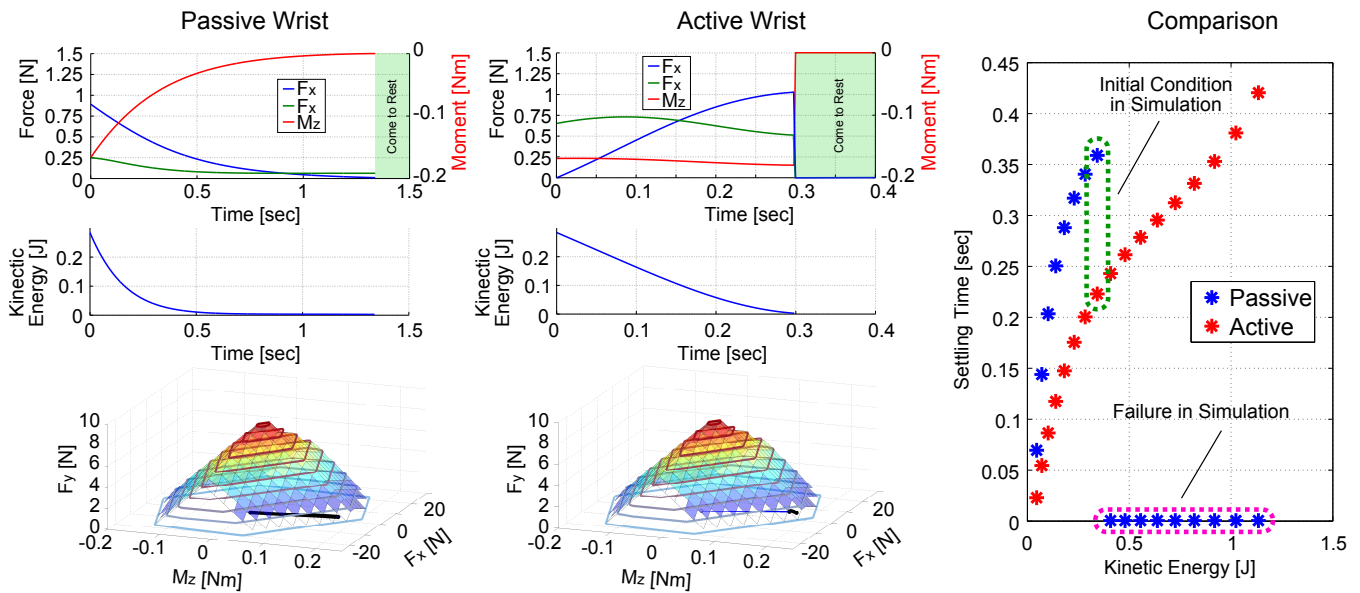


Fig. 8. Numerical simulation comparing a passive wrist with and active wrist for arresting a moving object. **Left:** The passive wrist represents the best case spring/damping values simulated for the chosen incoming speed. **Middle:** The active wrist uses the control law proposed in IV, applying forces proportional to the object’s momentum. **Right:** Settling time is shown as as the object comes in with different kinetic energy. While the active control is able to handle higher speeds, the tuned passive wrist quickly exerts forces higher than the adhesives’ capabilities and fails.

Forces/moments are shown to lie within the predicted limit surface for the successful grasp, whereas the failed grasp exceeds the limit and results in an adhesive failure. In the failed case, the incoming object had a higher kinetic energy, which produced larger wrist deflections that ultimately reached the joints’ range of motion. At this point, the interaction forces increased beyond the adhesive limits.

### C. Numerical Simulation of Dynamic Catch for Passive vs. Active Wrist

A numerical simulation compares the dynamic performance between a passive and an active wrist assumed to be attached to a gripper with the limit surface measured in section V-A. The two wrists simulated were:

- 1) A passive wrist of the same design as section III. Spring/damping constants optimized for settling time of catching the incoming object at speed  $\vec{v}_{sim}$  in order to represent a best case scenario.
- 2) An active wrist utilizing the active control law proposed in section IV with the gripper constraints measured in section V-A, exerting an opposing force proportional to the object’s momentum.

The passive wrist’s joint stiffness and damping constants were determined through an exhaustive search, though enforcing the natural frequency and damping ratio to be identical at each joint. Coefficients were chosen that minimized the time required to dissipate the kinetic energy to 2% of the object’s original energy, with initial velocity  $\vec{v}_{sim}$ . This resulted in a high level of damping at  $b_x = b_y = 1.2 N s/m$ ,  $b_\theta = 0.027 Nms$  and spring constants  $k_x = k_y = 0.39 N s/m$ ,  $k_\theta = 8.3 * 10^{-3} Nms$ , corresponding to  $\omega_n = 0.5 rad/sec$  and  $\zeta = 0.8$ .

The dynamic model tracked the state of a single rigid body being arrested by the forces exerted by each wrist. The simulation assumed the object started a given initial velocity, and was located within the gripper’s hold, with the wrist at its nominal resting position. In both cases, the simulated object had initial velocity oriented away from the gripper with appreciable spin:

$$\vec{v}_{sim} = \begin{bmatrix} 0 m/s & \hat{n}_x \\ -0.2 m/s & \hat{n}_y \\ 2\pi rad/s & \hat{n}_z \end{bmatrix}$$

The simulation results in Fig. 8 show that the ability to operate closer to the adhesive’s limits does yield benefit; the active wrist brings the object to rest in 59% of the time it takes for the passive wrist.

The comparison in the third column of Fig. 8 shows the time to slow the object’s motion as the initial energy is varied. For this sweep, components of the velocity are kept proportional as  $\vec{v}_{sim}$  is multiplied by a scalar. The active wrist is able adapt to the object’s higher initial velocity, whereas the passive wrist exceeds the adhesion’s capabilities for any higher velocities due to the high level of damping. Ultimately, factors such as the wrist’s range of motion will limit the ability to catch an object in either case, but are not considered here.

## VI. CONCLUSIONS AND FUTURE WORK

A model using grasp optimization was presented and compared to empirical measurements taken from a flexible gripper equipped with gecko-inspired, dry adhesive. The model was shown to be capable of evaluating the performance of different gripper geometries and adhesion capabilities. Adding a compliant wrist allowed the gripper

to grasp objects dynamically, applying moments in addition to forces.

To avoid overloading the adhesives with a sharp impulse, joints are allowed to deflect to transmit interaction forces across a longer amount of time. The adhesive limit surface was shown to be the deciding factor in determining the success or failure of grasping maneuvers.

Section III showed how tuning a passive, compliant wrist and gripper represents a compromise between limitations in different directions. Clever mechanism design, such as coupling compliance between axes, could lead to a better utilization of attainable forces with passive mechanisms. The mechanism presented here was designed to be easily tunable, with stiffnesses in orthogonal directions.

Active control was shown to outperform a passive gripper in a basic simulation presented in section V-C because forces and moments could be commanded as a function of one another. The ability to choose an operating point with respect to gripper limitations broadens both the magnitude and direction of forces/moments the gripper can exert.

This work leads to a number of future research directions. The active wrist algorithm proposed in section IV instantaneously optimizes an objective in order to slow down a moving object. More sophisticated methods could sacrifice slowing down the object for some duration in order to orient the gripper in a favorable position to apply larger forces, resulting in a more aggressive maneuver.

Free flyer manipulation is just one instance of a dynamical system where aggressive maneuvers are limited by the interaction forces that can be exerted. In this regard, grappling dynamic objects with an adhesive gripper is similar to the handling of race cars at the limits of their tires' friction cone [22]. Active control laws using force-constrained manipulators may entail planning a trajectory of forces/torques within or along surfaces representing limits of adhesion, friction, etc. The understanding of such limits will be used to expand free flyer dynamic grasping envelopes [11] and design approach maneuvers.

#### ACKNOWLEDGMENTS

This work was partially supported by NASA under the Space Technology Research Grants Program, Grant NNX12AQ43G and Early State Innovations Grant NNX16AD19G. Additional support was provided by NSF IIS-1161679 and ARL MAST MCE 14-4. M. Estrada is supported by the NSF Graduate Research Fellowship. The authors thank Roshena McPherson for stimulating discussions on gripper modeling, Shameek Ganguly for insights into active control using adhesion constraints, and Paul Mitiguy for consultation of the dynamics in section IV. The CAD model of SPHERES free flyer robot depicted in Fig. 1 was provided by the MIT Space Systems Laboratory.

#### REFERENCES

- [1] M. Bualat, J. Barlow, T. Fong, C. Provencher, T. Smith, and A. Zuniga, "Astrobee: Developing a free-flying robot for the international space station," in *AIAA SPACE 2014 Conference and Exposition*, vol. 4643, 2015.
- [2] T. Fong, M. Micire, T. Morse, E. Park, C. Provencher, V. To, D. Wheeler, D. Mittman, R. J. Torres, and E. Smith, "Smart spheres: a telerobotic free-flyer for intravehicular activities in space," in *Proc. AIAA Space*, vol. 13, 2013.
- [3] K. Yoshida, "Engineering test satellite vii flight experiments for space robot dynamics and control: theories on laboratory test beds ten years ago, now in orbit," *The International Journal of Robotics Research*, vol. 22, no. 5, pp. 321–335, 2003.
- [4] M. Henrey, J. Tellez, K. Wormnes, L. Pambaguian, and C. Menon, "Sticking in space: manufacturing dry adhesives and testing their performance in space environments," in *12th Symp. on Adv. Space Technologies in Robotics and Automation*, 2013, pp. 15–17.
- [5] C. Menon, M. Murphy, F. Angrilli, and M. Sitti, "Waalbots for space applications," in *55th Int. Astronautical Congress*, 2004.
- [6] A. Parness, T. Hilgendorf, P. Daniel, M. Frost, V. White, and B. Kennedy, "Controllable on-off adhesion for earth orbit grappling applications," in *IEEE Aerospace Conference*. IEEE, 2013, pp. 1–11.
- [7] D. Ruffatto, A. Parness, and M. Spenko, "Improving controllable adhesion on both rough and smooth surfaces with a hybrid electrostatic/gecko-like adhesive," *Journal of The Royal Society Interface*, vol. 11, no. 93, p. 20131089, 2014.
- [8] K. Yoshida, H. Nakanishi, H. Ueno, N. Inaba, T. Nishimaki, and M. Oda, "Dynamics, control and impedance matching for robotic capture of a non-cooperative satellite," *Advanced Robotics*, vol. 18, no. 2, pp. 175–198, 2004.
- [9] D. N. Nenchev and K. Yoshida, "Impact analysis and post-impact motion control issues of a free-floating space robot subject to a force impulse," *IEEE Transactions on Robotics and Automation*, vol. 15, no. 3, pp. 548–557, 1999.
- [10] A. Parness, "Anchoring foot mechanisms for sampling and mobility in microgravity," in *Robotics and Automation (ICRA), 2011 IEEE International Conference on*. IEEE, 2011, pp. 6596–6599.
- [11] M. A. Estrada, B. Hockman, A. Bylard, E. W. Hawkes, M. R. Cutkosky, and M. Pavone, "Free-flyer acquisition of spinning objects with gecko-inspired adhesives," in *2016 IEEE International Conference on Robotics and Automation (ICRA)*. IEEE, 2016, pp. 4907–4913.
- [12] M. Buss, H. Hashimoto, and J. B. Moore, "Dextrous hand grasping force optimization," *IEEE Transactions on Robotics and Automation*, vol. 12, no. 3, pp. 406–418, 1996.
- [13] L. Han, J. C. Trinkle, and Z. X. Li, "Grasp analysis as linear matrix inequality problems," *IEEE Transactions on Robotics and Automation*, vol. 16, no. 6, pp. 663–674, 2000.
- [14] R. Suárez, J. Cornella, and M. R. Garzón, *Grasp quality measures*. Institut d'Organització i Control de Sistemes Industrials, 2006.
- [15] P. Cheng, J. Fink, V. Kumar, and J.-S. Pang, "Cooperative towing with multiple robots," *Journal of mechanisms and robotics*, vol. 1, no. 1, p. 011008, 2009.
- [16] D. Santos, B. Heyneman, S. Kim, N. Esparza, and M. R. Cutkosky, "Gecko-inspired climbing behaviors on vertical and overhanging surfaces," in *Robotics and Automation, 2008. ICRA 2008. IEEE International Conference on*, May 2008, pp. 1125–1131.
- [17] P. Boscariol, M. A. Henrey, Y. Li, and C. Menon, "Optimal gait for bioinspired climbing robots using dry adhesion: a quasi-static investigation," *Journal of Bionic Engineering*, vol. 10, no. 1, pp. 1–11, 2013.
- [18] E. W. Hawkes, H. Jiang, and M. R. Cutkosky, "Three-dimensional dynamic surface grasping with dry adhesion," *International Journal of Robotics Research*, 2015.
- [19] A. L. Desbiens, A. T. Asbeck, and M. R. Cutkosky, "Landing, perching and taking off from vertical surfaces," *International Journal of Robotics Research*, 2011.
- [20] M. D. Lichter and S. Dubowsky, "State, shape, and parameter estimation of space objects from range images," in *Robotics and Automation, 2004. Proceedings. ICRA'04. 2004 IEEE International Conference on*, vol. 3. IEEE, 2004, pp. 2974–2979.
- [21] E. W. Hawkes, D. L. Christensen, A. K. Han, H. Jiang, and M. R. Cutkosky, "Grasping without squeezing: Shear adhesion gripper with fibrillar thin film," in *Proc. IEEE Conf. on Robotics and Automation*. IEEE, 2015, pp. 26–30.
- [22] K. Kritayakirana and J. C. Gerdes, "Autonomous vehicle control at the limits of handling," *International Journal of Vehicle Autonomous Systems*, vol. 10, no. 4, pp. 271–296, 2012.